An Alternative Formulation for the Empirical Mode Decomposition

Thomas Oberlin
Laboratoire Jean Kuntzmann,
University of Grenoble and CNRS, France
Tel:0033-4-76-51-45-61
E-mail: thomas.oberlin@imag.fr

Sylvain Meignen
Laboratoire Jean Kuntzmann,
University of Grenoble and CNRS, France
Tel:0033-4-76-51-43-95
FAX:0033-4-76-63-12-63
E-mail: sylvain.meignen@imag.fr

Valérie Perrier
Laboratoire Jean Kuntzmann,
University of Grenoble and CNRS, France
Tel:0033-4-76-51-45-51
FAX:0033-4-76-63-12-63
E-mail: valerie.perrier@imag.fr

Abstract- The Empirical Mode Decomposition (EMD) is a relatively new adaptive method for multicomponent signal representation which allows for analyzing nonlinear and non-stationary signals. In spite of its lack of mathematical foundations, very few papers are dedicated to defining new decompositions that would preserve the interesting properties of the EMD while improving the mathematical setting. The new decomposition based on direct constrained optimization we introduce in this article is an attempt in that direction.

Keywords- EMD, Constrained optimization, Adaptive signal decomposition
EDICS Category: DSP-TFSR, DSP-MULT

I. Introduction

The now well known Empirical Mode Decomposition (EMD), introduced by Huang et al. [1], is a data-driven signal processing method aiming at recovering the original AM/FM components (called Intrinsic Mode Functions (IMFs)) of a multicomponent signal. Due to its ability to deal with non-stationarities and nonlinearities, the EMD is widely used in signal processing [2], [3]. However, the sifting procedure (SP) computing the IMFs is based on ad hoc parameters and lacks mathematical foundations. Recently, variants of the SP, based either on partial differential equations [4], [5] or optimization methods [6], [7], have been proposed, providing a better mathematical framework. Nevertheless, this improvement is often achieved to the detriment of the interesting properties of the EMD.

The present paper introduces a new EMD-like decomposition where a constrained optimization step replaces the SP. Our goal is to show that it reproduces (or even improves) the behavior of the EMD but in a much clearer mathematical setting. After a brief overview of the EMD and its properties in section II, the new decomposition is detailed in section III. Section IV discusses the sensitivity of the new decomposition to its parameters. The beginning of section V is devoted to illustrations of the proposed method and then comparisons with the EMD on controlled situations. This enables us to obtain quantitative measures of the quality of the decomposition. We finally address the noise issue to conclude that one had rather denoise the signal before decomposing it. In this regard, we also put the emphasis on the SP working on its initialization. This enables us to obtain meaningful modes even in a noisy context.

II. Empirical Mode Decomposition

The EMD aims at decomposing a multicomponent signal $s(t)$ into a number J of so-called IMFs $h_j(t)$, $1 \leq j \leq J$:

$$s(t) = \sum_{j=1}^{J} h_j(t) + r(t), \tag{1}$$

where the modes h_j oscillate decreasingly with increasing j, and r is a monotonic residue. In this context, an IMF is defined as an oscillating function having a symmetric envelope.

Each IMF h_j is computed from m_{j-1} defined by:

$$m_j(t) \quad = \quad \begin{cases} s(t), & j = 0 \\ s(t) - \sum_{i=1}^{j} h_i(t), & j \geq 1. \end{cases} \tag{2}$$

The computation of the IMF h_j from m_{j-1} is carried out through a sifting procedure (SP) which defines h_j as the limit of the following sequence $(h_j^n)_{n\geq 0}$:

$$\left\{\begin{array}{rcl} h_j^0 & = & m_{j-1} \\ h_j^{n+1} & = & h_j^n - \frac{E_{\max}(h_j^n)+E_{\min}(h_j^n)}{2} := \phi(h_j^n), \end{array}\right. \tag{3}$$

where the so-called upper envelope $E_{\max}(h_j^n)$ (resp. lower envelope $E_{\min}(h_j^n)$) is the cubic spline interpolant to h_j^n at its local maxima (resp. minima). In practice, the SP stops when an ad hoc stopping criterion is met, leading to the IMF h_j. This criterion can be of Cauchy-type [1] or related to the symmetry of the envelope [8]. In most cases, the SP produces modes $(h_j)_{1\leq j\leq J}$ having an approximately symmetric envelope but there exist serious limitations to this approach. First, the symmetry of the envelope, in a cubic spline interpolation framework, would imply that the upper and the lower envelopes of h_j are cubic polynomials on the whole time span [9]. Second, given a stopping criterion and a signal, there is no reason why the SP should stop in a finite number of steps.

When it works, the EMD computes h_j from m_{j-1} and then m_j from m_{j-1} and h_j through:

$$m_j = m_{j-1} - h_j. \tag{4}$$

In that context, h_j corresponds to the level-j detail while m_j is the level-j mean. The above definition of the EMD shows that it is a nonlinear multiscale adaptive decomposition which is known to satisfy the two following properties:

- it behaves on average like a dyadic filter bank [10],
- it is a *quasi-orthogonal* decomposition [1], i.e., the modes $(h_j)_{1\leq j\leq J}$ are almost orthogonal.

Even if these properties are of empirical nature, they have greatly contributed to the success of the EMD and should be kept in mind when introducing new methods for modes computation.

III. Optimization-Based EMD for Multicomponent Signals

In this section, we propose a new EMD-like multicomponent signal decomposition. We show that, by replacing the SP by a constrained optimization procedure, the problem of the determination of the modes becomes solvable. In our framework, instead of determining the mode h_j from m_{j-1} as the SP does, we had rather estimate m_j from m_{j-1} and then deduce h_j using (4). Note that the method has the same recursive structure as the EMD. Indeed, one first extracts the level-1 mean m_1 from the signal s and then deduce the level-1 detail h_1, the procedure is then repeated on m_1, and so on. For that reason, we only need to describe the computation of level-1 mean and detail, denoted by m and h hereafter, from s.

More precisely, we split the signal s into the level-1 mean m, plus a level-1 detail, h, by beginning with an estimate $\hat{m}$ of m and then finding m by a constrained optimization problem that forces the detail curve h to have approximately symmetric envelopes. The calculation of m from s consists of two steps:

- Compute an estimate $\hat{m}$ of m in Π_τ^k the spline space of order k defined on some knot sequence τ (see section III-A).
- Search for m in $C(\hat{m})$, a non-empty closed convex set of Π_τ^k, by solving the quadratic optimization problem:

$$m = \underset{\tilde{m}\in C(\hat{m})}{\operatorname{argmin}} \left\| \tilde{m}^{(2)} \right\|^2, \tag{5}$$

where $\|.\|$ is the classical L^2 norm and where the closed convex set $C(\hat{m})$ is defined by linear constraints on $\tilde{m}$ which tend to force h to have an approximately symmetric envelope (see section III-B). The notation $m^{(n)}$ denotes the nth derivative of the one-dimensional function m.

Remark: Among all splines in the set of constraints $C(\hat{m})$, the optimizer chooses the smoothest one. Note also that this choice for the minimization functional imposes that $k \geq 3$.

A. Computation of the Estimate $\hat{m}$

Let $\hat{x} = (\hat{x}_i)_{1\leq i\leq L}$ be a vector estimating the location of the extrema x_i of h. It is most commonly chosen to be equal to the location of the extrema of s, but can be of other types, as explained later in section III-C. To build the estimate $\hat{m}$, we compute, as in [11], the points $(\bar{t}_i, \bar{s}_i)_{i=1\ldots L-1}$ by:

$$\begin{aligned} \bar{s}_i &= \frac{1}{\hat{x}_{i+1} - \hat{x}_i} \int_{\hat{x}_i}^{\hat{x}_{i+1}} s(t)\ dt \\ \bar{t}_i &= \frac{\int_{\hat{x}_i}^{\hat{x}_{i+1}} t|s(t) - \bar{s}_i|^2\, dt}{\int_{\hat{x}_i}^{\hat{x}_{i+1}} |s(t) - \bar{s}_i|^2\, dt}, \end{aligned} \tag{6}$$

and also boundary point $(\bar{t}_0, \bar{s}_0)$ (resp. $(\bar{t}_L, \bar{s}_L)$), as the symmetrical point of $(\bar{t}_1, \bar{s}_1)$ (resp. $(\bar{t}_{L-1}, \bar{s}_{L-1})$) with respect to $\hat{x}_1$ (resp. $\hat{x}_L$). $\bar{s}_i$ is the mean value of s on the interval $[t_i, t_{i+1}]$, while $\bar{t}_i$ is the time barycenter. $\hat{m}$ will finally be a spline of order k interpolating these $L+1$ points and defined on some knot sequence $\tau = (\tau_i)_{0\leq i\leq L+k}$, i.e., $\hat{m}$ is a piecewise polynomial of degree $k-1$ on the intervals bounded by the knot sequence τ having global regularity $\mathcal{C}^{k-2}$.

We need to define the knot sequence τ from $\bar{t}$ to ensure the existence and the uniqueness of the spline interpolant. Such a knot sequence τ can be obtained using the classical definition of DeBoor [12]:

- multiple knots are defined at boundary points: $\tau_0 = \ldots = \tau_{k-1} = \bar{t}_0$ and $\tau_{L+1} = \ldots = \tau_{L+k} = \bar{t}_L$,

- and single knots elsewhere:

$$\forall i \in k \dots L,\ \tau_i = \frac{1}{k-1} \sum_{p=i+1-k}^{i-1} \bar{t}_p. \tag{7}$$

Now, let us consider $N_{i,\tau}^k$, the i^{th} B-spline function of order k defined on the subdivision τ and supported on $[\tau_i, \tau_{i+k}]$. Since (7) implies that $\forall i \in 0, \dots, L,\ N_{i,\tau}^k(\bar{t}_i) > 0$, the Schoenberg-Whitney theorem ensures the existence of a unique spline interpolant $\hat{m}$ of order k at $(\bar{t}_i, \bar{s}_i)_{0 \le i \le L}$ (see for example [13]).

B. Computation of m

Referring to (5), the definition of the level-1 mean m requires the knowledge of τ and the set of constraints $C(\hat{m})$ on which we now focus. The motivation supporting the design of the set $C(\hat{m})$ is that the envelope of h should approximately be symmetric. Let us now detail the linear constraints that make up $C(\hat{m})$. Recall that $x = (x_i)_{1 \le i \le L}$ is the vector of the location of the extrema of h and let λ_i be the ordinate associated with x_i on the segment delimited by $(x_{i-1}, h(x_{i-1}))$ and $(x_{i+1}, h(x_{i+1}))$ (see Figure 1, for an illustrative example):

$$\lambda_i = \frac{h(x_{i+1}) - h(x_{i-1})}{x_{i+1} - x_{i-1}}(x_i - x_{i-1}) + h(x_{i-1}), \tag{8}$$

which is only valid for $i = 2, \cdots, L-1$. To define λ_1 and λ_L, we extend the signal by mirror

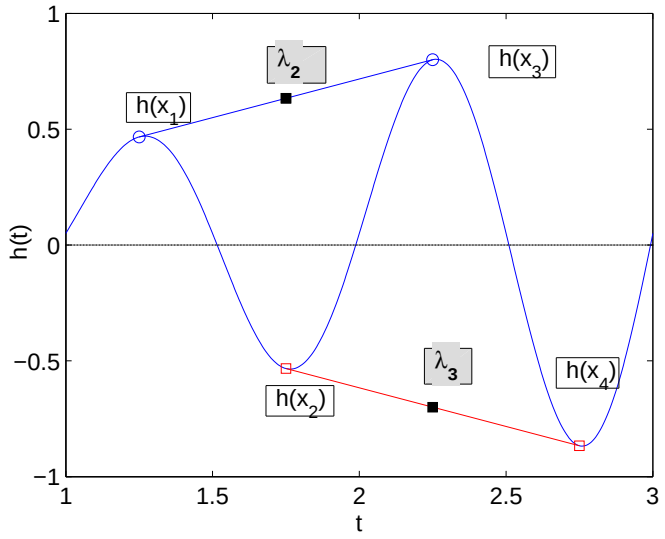

Fig. 1: Definition of λ_2 and of λ_3

extension with respect to the points $(x_1, h(x_1))$ and $(x_L, h(x_L))$ and then define $(x_0, h(x_2))$ (resp.

$(x_{L+1}, h(x_{L-1}))$), the symmetrical point of $(x_2, h(x_2))$ (resp. $(x_{L-1}, h(x_{L-1}))$). We finally get λ_1 and λ_L by applying (8) to the extended set $\{(x_0, h(x_2)), (x_i, h(x_i))_{1\leq i\leq L}, (x_{L+1}, h(x_{L-1}))\}$.

Bearing in mind the symmetry of the envelope of h, we seek constraints on h of the following kind:

$$|h(x_i) + \lambda_i| \leq \varepsilon_i. \tag{9}$$

Indeed, assume $h(x_i)$ is a maximum (resp. minimum) for h, then $(x_i, h(x_i))$ belongs to the upper (resp. lower) envelope of h, while (x_i, λ_i) belongs to the affine interpolant to the lower (resp. upper) envelope of h. As h should ideally have a symmetric envelope, this motivates (9). As the threshold ε_i ought to depend on the local amplitude of h, it is natural to choose $\varepsilon_i = \alpha\,|h(x_i) - \lambda_i|$, where α is a global parameter. Note that if h has an approximately symmetric envelope, $|h(x_i) - \lambda_i|$ approximates twice the amplitude of h. Finally, the sought constraints can be written in the form:

$$|h(x_i) + \lambda_i| \leq \alpha |h(x_i) - \lambda_i|. \tag{10}$$

To linearize these constraints on h, we replace x by $\hat{x}$ whenever it appears in (10) and h and λ_i by their estimates $s - \hat{m}$ and $\hat{\lambda}_i$ on the right hand side of (10). Defining:

$$\hat{\lambda}_i(m) = \frac{(s-m)(\hat{x}_{i+1}) - (s-m)(\hat{x}_{i-1})}{\hat{x}_{i+1} - \hat{x}_{i-1}}(\hat{x}_i - \hat{x}_{i-1}) + (s-m)(\hat{x}_{i-1}), \tag{11}$$

the new constraints can be written as

$$|(s-m)(\hat{x}_i) + \hat{\lambda}_i(m)| \leq \alpha |(s-\hat{m})(\hat{x}_i) - \hat{\lambda}_i(\hat{m})|. \tag{12}$$

These define the set of constraints $C(\hat{m})$ and enable us to rewrite the optimization problem, defined in (5), in the following form:

$$m = \begin{cases} \underset{\tilde{m}\in C(\hat{m})}{\operatorname{argmin}} \left\|\tilde{m}^{(2)}\right\|^2 \\ C(\hat{m}) = \left\{\tilde{m} \in \Pi_\tau^k,\ \forall i \in 1 \dots L,\ \ \frac{|\hat{\lambda}_i(\tilde{m}) + (s-\tilde{m})(\hat{x}_i)|}{|\hat{\lambda}_i(\hat{m}) - (s-\hat{m})(\hat{x}_i)|} \leq \alpha \right\}. \end{cases} \tag{13}$$

Let us note that the functional we minimize is quadratic and can be written as $M^T H M$, where M is the coefficients matrix of m in the B-spline basis $(N_{i,\tau}^k)_i$ and H is the stiffness matrix defined by $H_{iq} = \int_0^1 (N_{i,\tau}^k)''(t)(N_{q,\tau}^k)''(t)\,dt$.

Theorem 1: For $\alpha \geq 0$, the problem (13) has a unique solution m.

Proof: As the functional is quadratic, it suffices to show that $C(\hat{m})$ is convex and non-empty. The convexity comes from the fact that $C(\hat{m})$ is a convex polyhedron (defined by linear constraints). Hence the uniqueness of the solution. Then, $C(\hat{m})$ is non-empty if there exists a spline $\tilde{m}$ in Π_τ^k such that

$$\hat{\lambda}_i(\tilde{m}) + (s - \tilde{m})(\hat{x}_i) = 0,\ i = 1, \dots, L. \tag{14}$$

As $\hat{\lambda}_i(\tilde{m})$ is a linear function of the vector $((s-\tilde{m})(\hat{x}_i))_{i=1,\dots,L}$ (see (11)), there exists a solution to (14) if

$$\tilde{m}(\hat{x}_i) = s(\hat{x}_i),\ i = 1, \dots, L. \tag{15}$$

We recall that, in section III-A, we constrained the knot sequence τ to satisfy: $\forall i \in 0, \dots, L,\ N^k_{i,\tau}(\bar{t}_i) > 0$. This relation implies: $\forall i \in 0, \dots, L,\ \tau_i \leq \bar{t}_i \leq \tau_{i+k}$. In addition, we have, by definition of $\bar{t}_i$, that $\forall i \in 1, \dots, L,\ \bar{t}_{i-1} < \hat{x}_i < \bar{t}_i$. It follows that for $i \in 1 \dots L$, either $N^k_{i-1,\tau}(\hat{x}_i) > 0$ or $N^k_{i,\tau}(\hat{x}_i) > 0$ and then, by the Schoenberg-Whitney theorem [13], there exists at least one spline $\tilde{m}$ interpolating $(\hat{x}_i, s(\hat{x}_i))_i$ and belonging to Π^k_τ, which proves (15), hence theorem 1.

■

C. Computation of the Estimate $\hat{x}$

To start with, we note that the estimate $\hat{x}$ is both used in the definition of $\hat{m}$ and of the convex set $C(\hat{m})$, making the quality of this estimate a key point of the proposed method. Let us recall that, in the EMD, $\hat{x}$ is the location of the extrema of s. The role of the SP is then to iteratively change this estimate to make it fit the location of the extrema of h. As our optimization formulation does not use any iterative procedure, our concern is to estimate directly, and with good accuracy, the location of the extrema of h.

As explained in [14], the location of the extrema of even-order derivatives of s are more likely to provide better estimates of that of h than that of s does. In [14], the estimation of the location of the extrema of h by that of $s^{(2)}$ is investigated when s is as follows:

$$s(t) = \sum_{i=1}^{J} a_i \cos(2 f_i \pi t),$$

where $a_i > 0$ and f_i is assumed to be decreasing with i. It is proved there, using a maximal deviation argument, that the location of the extrema of $s^{(2)}$ better estimates that of $s_1(t) = a_1 \cos(2 f_1 \pi t)$ than the extrema of s does. However, from a practical point of view, the maximal deviation may not be sufficiently informative. To argue upon this, one considers the following simple two-tone signal:

$$s(t) = \cos(2\pi t) + a \cos(2\pi f t) \quad 0 < f < 1,\ a \in \mathbb{R}^*_+. \tag{16}$$

As $f < 1$, the high-frequency tone is always $s_1(t) = \cos(2\pi t)$. If one refers to Proposition 1 of [15], when $af < 1$ the rate of extrema for s, i.e., the average number of extrema per second, is exactly the same as that for s_1, while when $af^2 > 1$ the rate of extrema for s is exactly the same as that for s_2 (which equals $a \cos(2\pi f t)$ here). This proposition can then be generalized to even higher-order derivatives: the

number of extrema of $s^{(2p)}$ equals that of s_1 (resp. s_2) when $af^{2p+1} < 1$ (resp. $af^{2p+2} > 1$). In spite of the proof of this proposition being very similar to that of Proposition 1 of [15], we recall it in Appendix A for the reader's convenience.

Now, assume that the number of extrema of s_1 is correctly estimated. The main observation that makes the estimate of the location of the extrema of s_1 better when using even higher-order derivatives of s is the following. Since

$$s^{(2p)}(t) = (-1)^p (2\pi)^{2p} \left(\cos(2\pi t) + af^{2p} \cos(2\pi f t)\right),$$

$s^{(2p)}$ looks like s, but with a low-frequency tone s_2 attenuated by a factor f^{2p}. As the attenuation factor decreases when p increases, the location of the extrema of s_1 is better estimated in that case. However, numerical instabilities are created by high-order differentiation, which is a strong restriction to its use. This remark leads us to build a trade-off procedure to determine a good order of differentiation to both estimate the number of extrema of s_1 and then locate them. This procedure consists of computing the smallest p such that $s^{(2p)}$ has supposedly the same number of extrema as s_1.

Let us denote by $t^{[0]}$ (resp. $t^{[2]}$, $t^{[4]}$) the location of the extrema of s (resp. $s^{(2)}$, $s^{(4)}$) and by $|X|$ the cardinality of any set X. The procedure to compute the estimate $\hat{x}$ is the following:

- if $|t^{[0]}| = |t^{[2]}|$, then $\hat{x} = t^{[0]}$,
- otherwise, if $|t^{[2]}| = |t^{[4]}|$ and $|t^{[2]}| > |t^{[0]}|$, then $\hat{x} = t^{[2]}$,
- otherwise, $\hat{x} = t^{[4]}$.

To compute the second-order derivative, we use its fourth-order approximation:

$$s^{(2)}(t) \approx \frac{-s(t-2\delta)+16s(t-\delta)-30s(t)+16s(t+\delta)-s(t+2\delta)}{12\delta^2}, \tag{17}$$

where δ is the sampling period. The fourth-order derivative is obtained by iterating this formula twice. At the boundaries, we use a shifted version of (17). Let us remark that δ must neither be too large, to prevent discretization errors, nor too small, to avoid numerical errors caused by the round-off unit. Note also that, to guard against potential sampling artifacts, we take the sampling rate to be at least equal to five times the Nyquist rate [16].

The results of this adaptive selection procedure of the differentiation order are displayed on Figure 2, for the signal defined in (16). Each color corresponds to a particular value for $\hat{x}$, i.e., either $t^{[0]}, t^{[2]}$ or $t^{[4]}$. Recalling that s_1 has as many extrema as s when $af < 1$, as many as $s^{(2)}$ when $af > 1$ and $af^3 < 1$, as many as $s^{(4)}$ when $af^3 > 1$ and $af^5 < 1$, we conclude that the selection procedure manages to find the number of extrema of s_1 in almost any cases if $af^4 < 1$. When $af^4 > 1$ the procedure finds as many extrema as s_2 and the first mode is not extracted. We shall finally mention that horizontal stripes

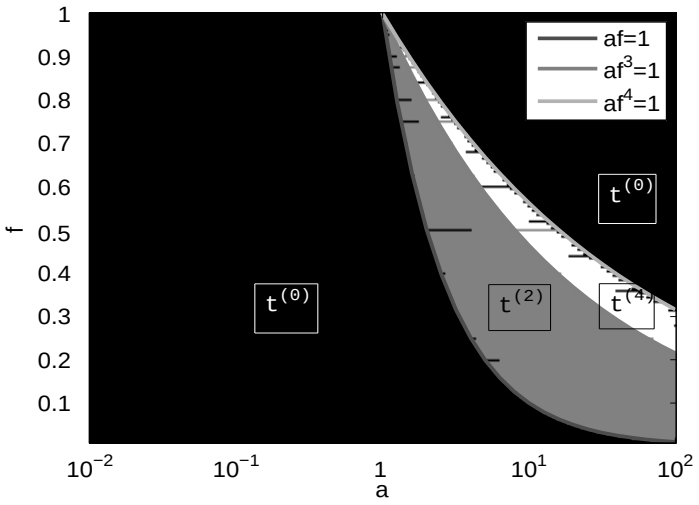

Fig. 2: Result of the procedure to determine the order of differentiation of s used to compute $\hat{x}$. From left to right, we display the regions where $\hat{x}$ equals $t^{[0]}$ (in black), $\hat{x}$ equals $t^{[2]}$ (in gray) or $\hat{x}$ equals $t^{[4]}$ (in white). The equations of the three curves are, from bottom-left to top-right: $af = 1$, $af^3 = 1$, $af^4 = 1$. These curves determine almost exactly the three different domains, except for some horizontal instabilities.

on Figure 2 stem both from the finiteness of the signal and numerical approximations in the computation of the derivative.

D. Discussion on the Method

From now on, we call *OS-decomposition* (OS meaning Optimization on Splines) the decomposition $(h_j)_{1\leq j\leq J}$ obtained by recursively applying the optimization procedure described in III-B. In the following $\hat{x}_j$, $\hat{m}_j$ and $C(\hat{m}_j)$ are obtained from m_{j-1} in the same way as $\hat{x}$, $\hat{m}$ and $C(\hat{m})$ from $m_0 = s$. Table I summarizes the differences between the OS-decomposition and the EMD. Let us now discuss some parameters of the optimization procedure.

1) Parameter α: The constraints, defined in (10), which force the symmetry of the mode h_j involve a parameter α. Relation (10) is very similar to the stopping criterion, proposed in [8], where the SP (see 3) stops when

$$\sigma(h_j^n)(t) = \frac{|E_{\max}(h_j^n)(t) + E_{\min}(h_j^n)(t)|}{|E_{\max}(h_j^n)(t) - E_{\min}(h_j^n)(t)|} \leq \alpha_{SP}, \tag{18}$$

OS-decomposition	EMD
Input : a signal s, a stop parameter α	
Output : the IMFs $h_1, h_2, \ldots, h_J$ and a residue r	
$m_0 := s; j = 0;$	
while m_j has more than 3 extrema repeat	**while** m_j has more than 3 extrema repeat
$j := j + 1$	$j := j + 1$.
Extraction of h_j : OS process	Extraction of h_j : Sifting Process
Estimation of the extrema $\hat{x}_j$ of h_j from m_{j-1}	Initialization $n := 0; h_j^n := m_{j-1};$
Building of the estimate $\hat{m}_j$ of m_j	**while** h_j^n is not an IMF do
Computation of the level-j mean m_j in a B-spline space	$h_j^{n+1} = \phi(h_j^n); n := n + 1;$
	$h_j = h_j^n;$
$h_j := m_{j-1} - m_j$	$m_j := m_{j-1} - h_j;$

TABLE I: Comparison between the OS-decomposition and the EMD.

is satisfied for some n and almost all t, typically for 95% of the signal duration. Here also the parameter α_{SP} controls the symmetry of h_j and seems very similar to our parameter α, but our approach is different in that the constraints are only verified at $\hat{x}_j$ and not at each time t. This point is essential to ensure that the set of constraints $C(\hat{m}_j)$ is non-empty (see Theorem 1). The sensitivity of the optimization procedure to the parameter α will be discussed in section IV-A.

2) The choice of the approximation space: B-splines are particularly well-adapted to our optimization procedure for the following reasons:

- to represent smooth functions using splines reduces the dimension of the space and fixes the optimization step,
- the advantage of B-splines over other parameterizations, such as piecewise Hermite interpolation, in the context of instantaneous frequency estimation has been pointed out in [17]. The authors show there that the Hilbert transform of B-splines is computed by a simple recursion formula.

Another important parameter is the spline order k. Indeed, after having applied the optimization procedure to s, the method restarts the process on the spline function m_1. If m_1 is a spline of order $k = 4$, i.e., a cubic spline, the estimation of the location of the extrema of h_2 using higher order of differentiation of m_1 is irrelevant, since $m_1^{(4)}$ is not meaningful. Thus, the order of the spline space used in the optimization step in the whole decomposition has to be larger or equal to 6.

3) The estimates $\hat{x}_j$ and $\hat{m}_j$: The motivation for the first estimate is related to the choice of imposing constraints at the extrema locations of h_j, while the second estimate is involved in the constraints linearization. We have already motivated the choice for $\hat{x}_j$, computed as in section III-C, by remarking that it enables to better determine the number and the location of the extrema of the first mode than the estimate used by the EMD does. The proposed construction for $\hat{m}_j$ based on the local integral computations was successfully used in the EMD context by Hong et al. [11]. To study the sensitivity of our method to this estimate, we have taken other definitions for $\hat{m}_j$ into consideration, section IV-B will present comparative results which show that the retrieval of the first mode is not sensitive to the choice of $\hat{m} = \hat{m}_1$.

IV. Sensitivity to the Parameters of the OS-Decomposition

We now address the issue of the sensitivity to the parameters of the OS-decomposition on model signals of the following kind:

$$s(t) = \sum_{i=1}^{J} s_i(t) := \sum_{i=1}^{J} a_i(t)\cos(\Phi_i(t))$$

such that for all t, $\Phi_i'(t) > \Phi_{i-1}'(t) > 0$ and $a_i(t) > 0$. Furthermore, we assume that at each t the different components do not interfere. A typical example of such a signal is shown on Figure 3 (A) along with its ideal time-frequency representation.

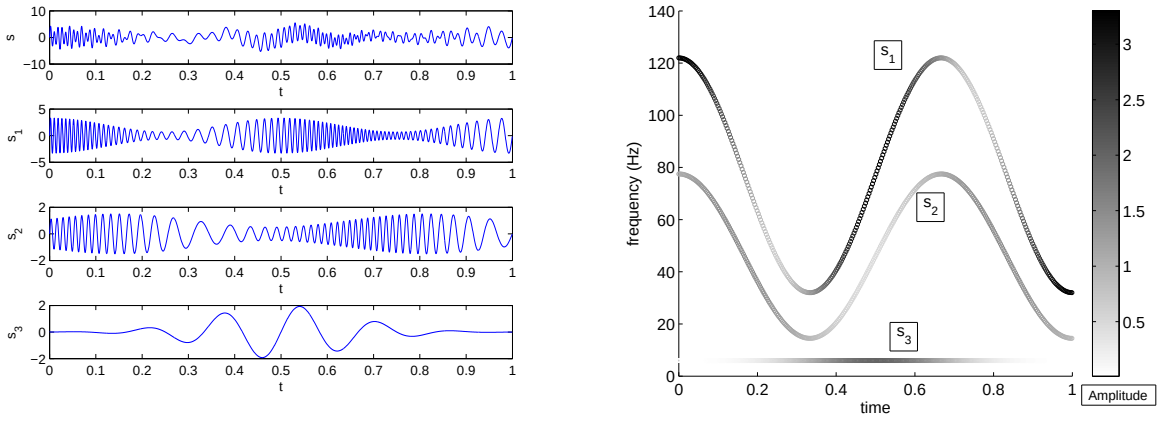

(A) (B)

Fig. 3: (A): the test signal s and its three components s_1, s_2, s_3, (B): the corresponding time-frequency representation of the components.

In the following simulations, we will compute the EMD as in [8], where the stopping criterion in the SP is based on two thresholds α_{SP} and β_{SP} which guarantee small global fluctuations of the computed level-j mean m_j, while enabling large local excursions. Considering the function σ defined in (18), this amounts to iterating the sifting until $\sigma(h_j)(t) < \alpha_{SP}$, for some prescribed fraction $1 - \gamma_{SP}$ of the total duration, while $\sigma(h_j)(t) < \beta_{SP}$ for the remaining fraction. The parameters retained for our simulations are $(\alpha_{SP}, \beta_{SP}, \gamma_{SP}) := (\alpha_{SP}, 10\,\alpha_{SP}, 0.05)$ as recommended by authors in [8]. For the sake of fair comparisons, we will set $\alpha_{SP} = \alpha$ in the following. Furthermore, $\hat{x}$, $\hat{m}$, h and m will still denote $\hat{x}_1$, $\hat{m}_1$, h_1 and m_1. Note that the Matlab code is available at [18], together with a script which creates the main figures of the paper.

A. Sensitivity of the Decomposition to the Parameters α and k

Here, we aim at numerically investigating the sensitivity of the OS-decomposition to the parameters α and k. For that purpose, we focus on the separation of the first mode from the rest of the signal. Let us denote by h_α the first mode obtained either by applying the EMD, computed as explained before, or the OS-decomposition for a given α. On Figure 4, we display the discrepancy between h_α and s_1 for the signal of Figure 3 (A), measured by the coefficient

$$C_1 = \log\left(\frac{\|s_1 - h_\alpha\|}{\|s\|}\right). \tag{19}$$

along with the variation rate $vr(\alpha)$ of h_α with respect to α defined by:

$$vr(\alpha) = \frac{\|h_{\tau_s+\alpha} - h_\alpha\|}{\tau_s}, \tag{20}$$

where τ_s is the discretization period. These coefficients are drawn as a function of the parameter α for different values of k.

Figure 4 (A) suggests an optimal value of α between 0.02 and 0.05 for the OS-decomposition for which the discrepancy between h_α and the expected mode s_1 is significantly smaller when the OS-decomposition is used instead of the EMD. According to Figure 4 (B), the variation rate has the same order of magnitude for both methods, and is more regular for the OS-decomposition than for the standard EMD. The spline order k does not seem to have much influence provided α is not too small: when $\alpha < 0.04$ the error as the variation rate of the solution is better when $k = 8$ or $k = 10$.

B. Sensitivity to the Estimate $\hat{m}$

The second major issue is the sensitivity of the optimization procedure to $\hat{m}_j$. Here, we study this issue by considering its influence on the retrieval of the first mode that is $j = 1$. The estimate $\hat{m}$ gives

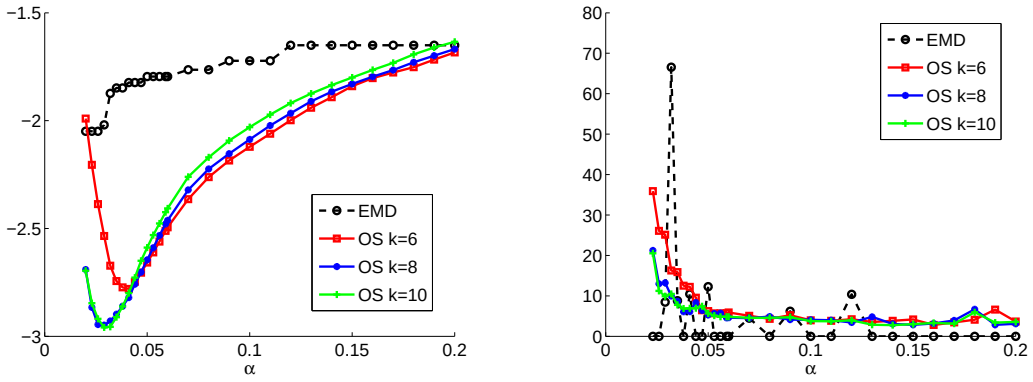

(A) (B)

Fig. 4: (A) : Coefficient C_1 as a function of α, for the test signal of Figure 3. (B) : the variation rate vr, defined in (20), as a function of α for the same signal. The results are given for the OS-decomposition with different spline orders k, and for the EMD.

access to two pieces of information regarding the optimization procedure:

- The subdivision τ associated with the definition of the spline space.
- An estimate $\hat{m}(\hat{x})$ of the amplitude of m at $\hat{x}$.

The subdivision τ does not influence the decomposition much, provided it is interwoven with the sequence $\hat{x}$ in such a way that Theorem 1 is valid. As for the influence of $\hat{m}(\hat{x})$ on the decomposition, given $\hat{x}$, we consider the following three possibilities to build this estimate:

1) The first one (called integral mean approach) described by equation (6) computes $\hat{m}(\hat{x})$ as the spline interpolant to $(\bar{t}_i, \bar{s}_i)_i$.
2) The second one (traditionally used in the EMD) constructs τ following equation (7), where τ_i is the middle of $[\hat{x}_i, \hat{x}_{i+1}]$ and then computes the upper (resp. lower) envelope as the cubic spline interpolant of s at $(\hat{x}_{2i})$ (resp. $(\hat{x}_{2i+1})$). Computing the half sum of these two envelopes, one gets the arithmetic mean $\hat{m}(\hat{x}) = m_e$.
3) The third one (B-spline approach) computes $\hat{m}$ following [17]. It is exactly the same procedure as the previous method, except that the arithmetic mean m_e is replaced by the definition given by equation (2.13) of [17] .

Setting $k = 8$, we then again compute the discrepancy between h_α and s_1 measured by the coefficient C_1 when one of the above estimate $\hat{m}(\hat{x})$ is used. The results of Figure 5 confirm that the proposed

method is slightly sensitive to this estimate.

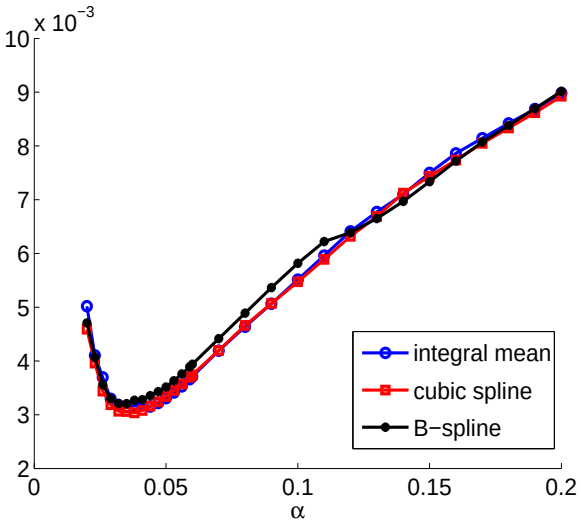

Fig. 5: Coefficient C_1 as a function of α, for the OS-decomposition using three different estimates $\hat{m}(\hat{x})$, for the test signal of Figure 3.

C. Sensitivity to the Parameters and Orthogonality Index

We here discuss the sensitivity of the decomposition to the parameters α and k as in section IV-A but using a different measure: the orthogonality index. Indeed, let us rate the orthogonality of the decomposition using the following orthogonality index:

$$io = \frac{1}{\|s\|^2} \sum_{1 \leq i < j \leq J} \langle h_i, h_j \rangle .$$

Figure 6 shows the orthogonality index io as a function of α computed for the signal of Figure 3 (so $J = 3$ in that case), for the OS-decomposition with different values of the spline order k and for the EMD. Note that the orthogonality index of the theoretical decomposition (s_1, s_2, s_3) is 3×10^{-3}.

We observe that io has similar values for all methods provided $k > 6$, which means that the order of the spline space has little impact on the decomposition when $k \geq 8$. For $k = 6$ the orthogonality index is quite high and oscillates a lot with α, because the method computing the estimate $\hat{x}$ using high order of differentiation of the signal is inaccurate in that case (see paragraph III-D2). An interesting phenomenon is that when α increases, the orthogonality index of the decomposition becomes much lower for the OS-decomposition than for the EMD. This comes directly from the definition of the functional in equation (5), as a high α means a large set of constraints $C(\hat{m})$.

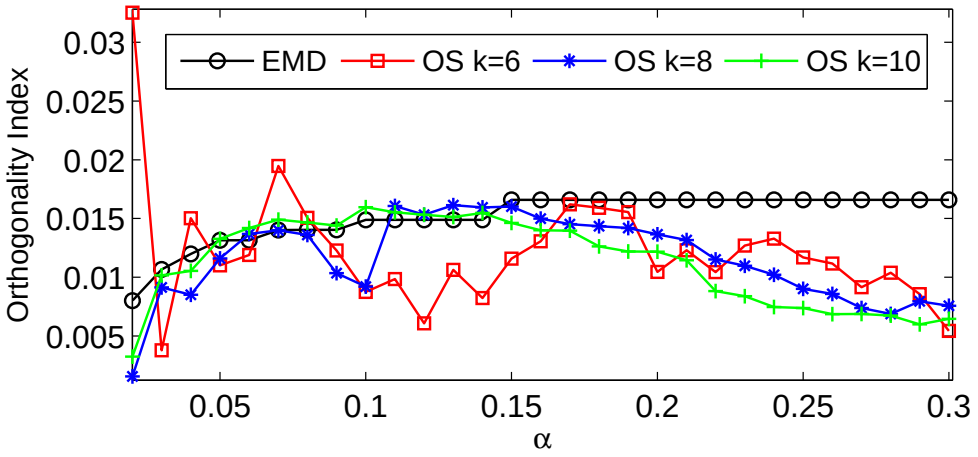

Fig. 6: The orthogonality index for the decomposition of the test signal (Fig. 3) into three components. io is plotted as a function of the parameter α, for the EMD and the OS-decomposition when the spline order is $k = 6$, $k = 8$, or $k = 10$.

V. Numerical Validation

In what follows, we first compare the OS-decomposition to the EMD computed as in [8], in terms of mode-mixing and narrow-band signal decomposition, still focusing on the retrieval of the first mode. We will then deal with the noise issue, but this time considering the whole decomposition. In order to highlight the importance of h_j^0 (see the definition (3) of the SP) in the EMD, we also study a slightly different version of the EMD, called "EMD-NI", obtained by putting $h_j^0 = m_{j-1} - \hat{m}_j$ in the initialization of the SP, where $\hat{m}_j$ is the estimate introduced in section III-A. In all the following tests the parameters involved in the OS-decomposition are set to $k = 8$ and $\alpha = 0.03$, or else we mention it. When the EMD or the EMD-NI are computed, the same value $\alpha_{SP} = \alpha$ is used and the extra parameters of these methods are defined as was previously.

A. Mode-mixing for two Tone-Signals

We first show how the adaptive choice of the differentiation order of s to estimate the extrema locations of s_1 improves the separation of the first mode $h = h_1$ from the rest of the signal. We again consider the simple two-tone signal defined in (16), and we measure the quality of the separation by computing the coefficient

$$C_2 = \frac{\|h - s_1\|}{\|s_2\|}. \tag{21}$$

This quantity has already been used in [15], and is similar to the coefficient C_1 except that s_2 replaces s as denominator. In fact, this modification allows us to better evaluate the method when a is small. When $C_2 \approx 0$ there is a good separation, whereas when $C_2 \approx 1$ the first mode has not been separated (in this case the method returns $h \approx s_1 + s_2$).

We compute the quantity C_2 as a function of a and f for the OS-decomposition, the EMD and the EMD-NI, the result being depicted on Figure 7 (A, B, C). These numerical results confirm the theoretical expectation for the OS-decomposition: the quality of the separation of s_1 from the rest of the signal is directly related to the estimate $\hat{x}$. We notice that the adaptive procedure used to define $\hat{x}$ in the OS-decomposition has a positive effect on the first mode separation, while the EMD, based on a poorer estimate $\hat{x}$, behaves worse with regards to this point. But, by changing the estimate $\hat{m}$ at the first iteration of the SP by the one proposed in section III-A (as in the EMD-NI does), the results are significantly improved. The comparison of Figures 7 (B) and (C) suggests that the EMD is very sensitive to the initialization of the SP. Furthermore, we should finally mention that stripes in the graphs of Figure 7 are associated with both the discrete nature of the stopping criterion and some numerical effects which we do not intend to analyze here.

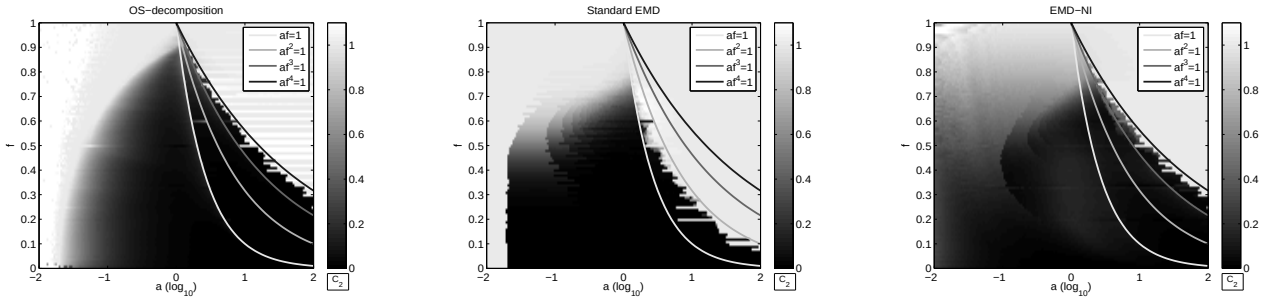

(A) (B) (C)

Fig. 7: Coefficient C_2 defined in (21) with respect to (a, f). $C_2 = 0$ (black areas) indicates that s_1 is correctly separated, while $C_2 \approx 1$ (white areas) means s_1 is not correctly separated. The results are given for the OS-decomposition (A), the EMD (B) and the EMD-NI (C).

B. Narrowband Signal Decomposition

Here, we compare the influence of the set of constraints $C(\hat{m})$, computed as defined previously or by the constraints introduced in [7], on the optimization procedure. Contrary to what is done in the present

paper, the constraints in [7] are both of equality and inequality types depending on the monotonicity of the upper and lower envelopes, and involve more criteria than the symmetry of the envelopes. To see in detail what these constraints are, we refer the reader to [7]. From now on, we will call EI-OS-decomposition (EI standing for "Equality Inequality"), the decomposition obtained by replacing the set of constraints in the OS-decomposition by those given in [7]. In addition, we compare the method to the standard EMD and the so-called "EMD-NI". For that purpose, we compute

$$C_1^n = \log\left(\frac{\|s_1 - h_1^n\|}{\|s\|}\right), \tag{22}$$

h_1^n being obtained after n sifting iterations on s in the EMD or in the EMD-NI. Of course, $n = 1$ for the OS-decomposition as for the EI-OS-decomposition method since they are not iterative. The results of Figure 8 show the convergence of the EMD to some h_1 which is definitely not s_1. We also notice that, while much better than the EMD, the EMD-NI method still gives a worse estimate of s_1 than the OS-decomposition does.

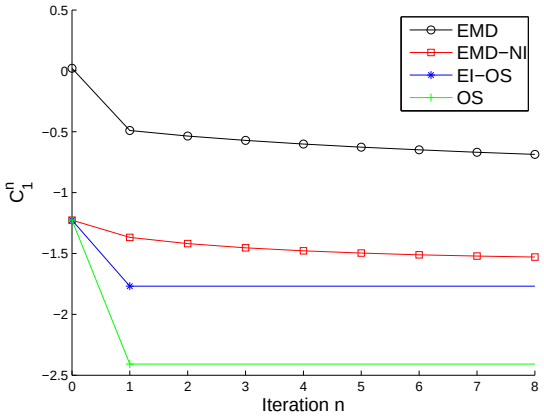

Fig. 8: Computation of (22) with four different methods, for the test signal s of Figure 3.

C. EMD and Noise

In this section, we discuss the noise issue in relation to the different decompositions. To start with, it is worth noting that the EMD was not designed to process noisy data. Indeed, the spreading of noise over several IMFs, often produces "mode-mixing effects", as shown in the example of Figure 10 (C), corresponding to the decomposition of the signal of Figure 9 (A).

The sensitivity to noise of the EMD makes the computation of the Hilbert spectrum very unstable. Different approaches have therefore been proposed to denoise the modes before computing the Hilbert spectrum either when the modes are associated with a wavelet decomposition [19] or produced by the EMD [20]. Rather, our approach here is to denoise the signal first and then to decompose it with the OS-decomposition or the EMD. Indeed, in a noisy context, all the discussion on the detection of the extrema location becomes irrelevant therefore we choose to proceed this way. In this regard, it would be of interest in a future work to compare these denoising strategies before or after decomposition in terms of the quality of the Hilbert spectrum.

To proceed as we do may appear a bit artificial but in many applications the denoising step and the analysis step are disconnected. In many cases, the signal is even low-pass filtered at an ad hoc frequency, that removes the major part of the noise. As an illustration, on Figure 9, we display a sum of two cosine functions with an additive Gaussian noise ($\sigma = 0.3$) along with its denoised version obtained via wavelet SURE-shrinkage (see [21]). Then, on Figure 10 (A) and (B), we display the decompositions of the denoised signal using the EMD and the OS-decomposition, respectively. In both cases, we obtain the cosine functions with small perturbations, and a very low orthogonality index. To compare with, the EMD of the noisy signal is also displayed on Figure 10 (C) clearly showing mode-mixing effect (the OS decomposition of the noisy signal would not lead to better results).

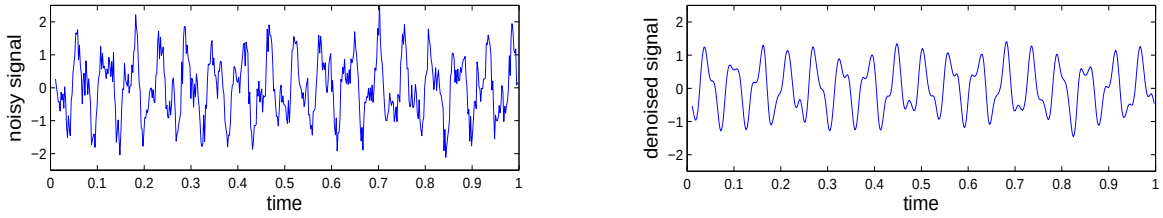

(A) (B)

Fig. 9: (A): noisy signal, a sum of cosines with a white Gaussian noise, $\sigma = 0.3$. (B): the signal after wavelet SURE-Shrinkage

D. Avoiding Mode-mixing by Using the EMD-NI

The mode-mixing phenomenon is inherent to the EMD and may arise in many instances other than noise. Several techniques such as the masking signal [22] or the Ensemble EMD [23] have been proposed to deal with this phenomenon. Here, our point is to show, on a example, how a better initialization of the

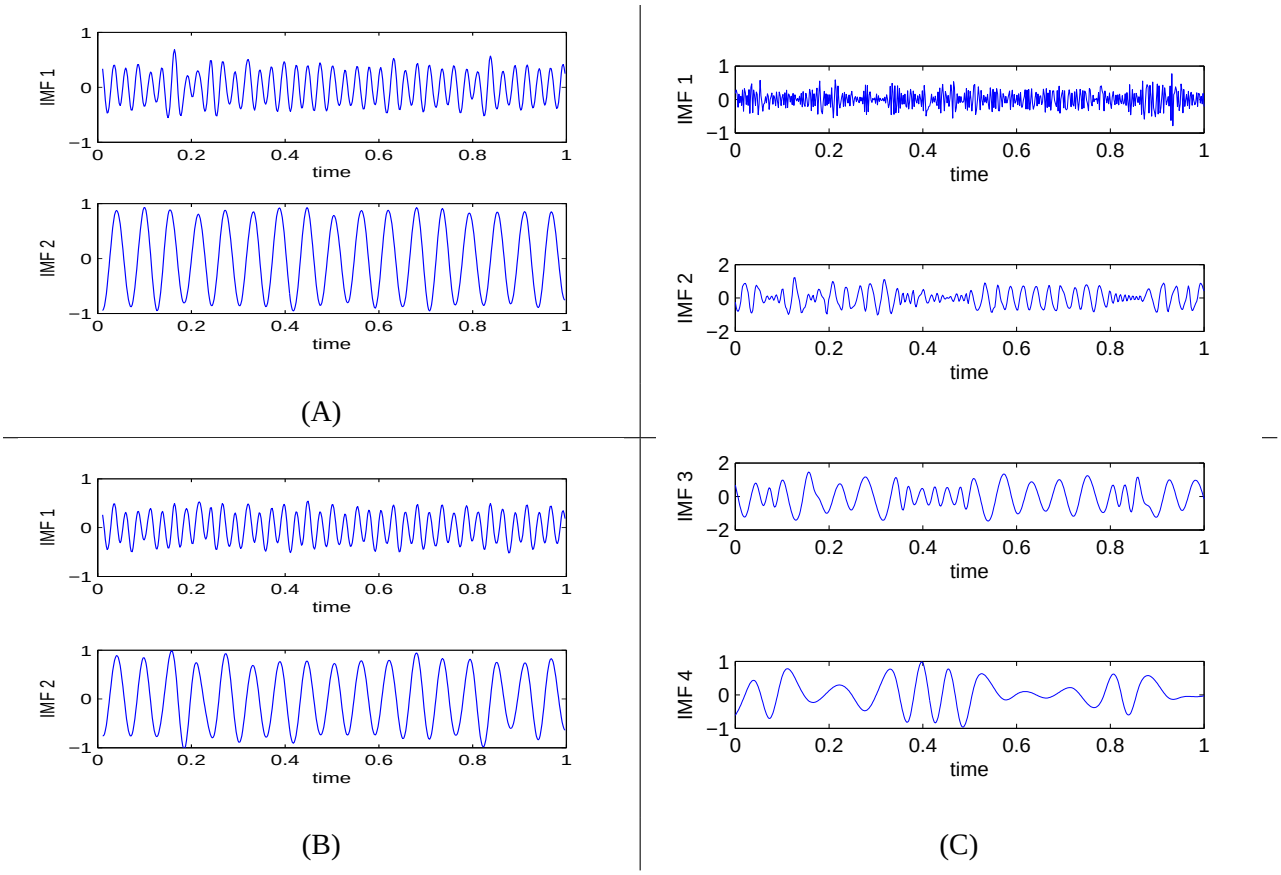

Fig. 10: (A): The denoised signal (Fig. 9 (B)) decomposed by EMD, the orthogonality index is $io = 0.017$. (B): same signal decomposed by OS, $io = 0.009$. (C): the original noisy signal of Fig. 9 (A) decomposed into 4 IMFs using the standard EMD, $io = 0.07$.

SP influences favorably the decomposition in terms of mode-mixing. Indeed, We compare the EMD-NI to the EMD for the signal of Figure 11 (A) made of the sum of s_1 and s_2 displayed on Figure 11 (B) plus an additive Gaussian noise ($\sigma = 0.4$). Looking at the EMD results on Figure 11 (C), the first IMF mainly contains noise for $t \in [0, 0.5]$ which is no longer the case in the second part of the signal where the amplitude of the noise is too small compared to that of the signal. As a consequence, the second and the third IMFs are meaningless. Unlike the EMD, the EMD-NI is relevant on this signal, as it leads to the first mode being the first IMF and the two following modes being those expected. Of course, some aspects of the method are not relevant here especially the procedure determining the location of the extrema of the first mode, and the reason for this much better behavior should be more deeply investigated. This example however shows the potential point of interest in working on the initialization of the SP to avoid

the mode-mixing problem.

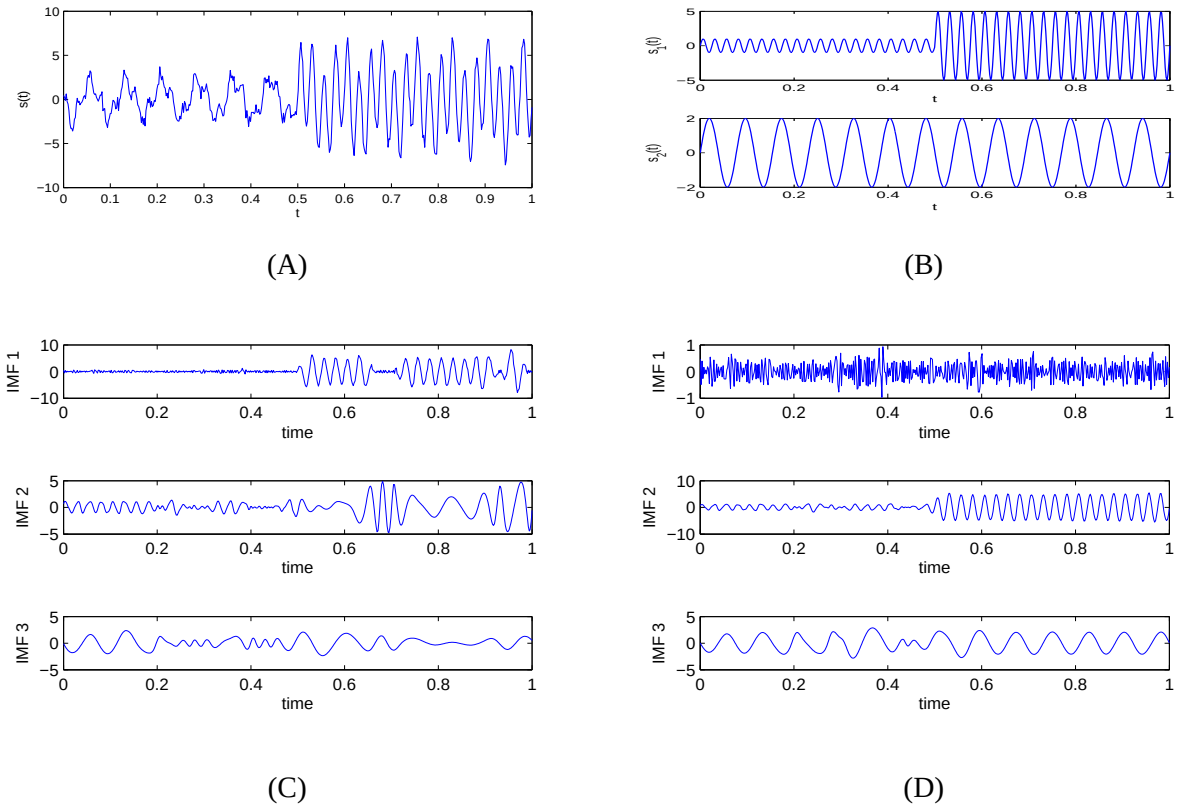

Fig. 11: (A): signal $s = s_1 + s_2$ plus Gaussian noise $\sigma = 0.4$. (B): the two components s_1 and s_2 of the signal. (C): the result of the EMD decomposition, the orthogonality index is $io = 0.09$. (D): the result of EMD-NI, $io = 0.007$. The method takes automatically $p = 2$ for the first IMF and $p = 0$ for the second and the third ones, in the computation of the estimate $\hat{x}$.

VI. Conclusion

In this paper, we have introduced a new signal decomposition based on constrained optimization. This decomposition offers an advantage over the EMD to make the computation of the modes solvable. After having studied the sensitivity of the method to its parameters, we have shown that it preserves the interesting properties of the EMD. For realistic signals corrupted by noise, the method is still efficient provided there is a denoising preprocessing step. Furthermore, we have also pointed out how sensitive the EMD is to initial conditions and we have proposed a small modification of the original algorithm which enables us to reduce the mode-mixing phenomenon. The generalization of this optimization approach

to the bidimensional case seems, at first sight, relatively straightforward: indeed, the constraints extend readily to interpolating functions on Delaunay triangulations, as used in [24]. This will therefore be the subject for further development.

APPENDIX A
PROOF OF THE EXTREMA REPARTITION

Let us recall the proposition of section III-C: consider the signal $s(t) = s_1(t) + s_2(t)$, with $s_1(t) = \cos(2\pi t)$ and $s_2(t) = a\cos(2\pi f t)$, for $a > 0$ and $0 < f < 1$. Then, the number of extrema of $s^{(2p)}$ equals the number of extrema of s_1 (resp. s_2) when $af^{2p+1} < 1$ (resp. $af^{2p+2} > 1$).

Proof: We first show that the sign of $s^{(2p+2)}$ at the location of the extrema of $s^{(2p)}$ is the same as that of $s_1^{(2p+2)}$ if $af^{2p+1} < 1$ and the same as that of $s_2^{(2p+2)}$ if $af^{2p+2} > 1$. Assuming that $s^{(2p)}$ admits an extremum at $t = t_0$, we want to show that:

$$\begin{aligned} |af^{2p+2}\cos(2\pi f t_0)| &< |\cos(2\pi t_0)| \text{ if } af^{2p+1} < 1 \\ |af^{2p+2}\cos(2\pi f t_0)| &> |\cos(2\pi t_0)| \text{ if } af^{2p+2} > 1. \end{aligned} \tag{23}$$

We first write

$$s^{(2p+1)}(t_0) = (-1)^{p+1}(2\pi)^{2p+1}\left(\sin(2\pi t_0) + af^{2p+1}\sin(2\pi f t_0)\right) = 0.$$

Then, squaring equation (23) and using the above relation, proving (23) amounts to determining the sign of

$$\gamma = a^2 f^{2(2p+2)}\cos^2(2\pi f t_0) + a^2 f^{2(2p+1)}\sin^2(2\pi f t_0) - 1.$$

If $af^{2p+1} < 1$ then $a^2 f^{2(2p+2)} < a^2 f^{2(2p+1)} < 1$ and $\gamma < 0$. Conversely, if $af^{2p+2} > 1$ then $a^2 f^{2(2p+2)} > a^2 f^{2(2p+1)} > 1$ and $\gamma > 0$, which proves (23).

As a result, $s^{(2p)}$ has exactly one extremum between two zero-crossings of $s_1^{(2p+2)}$ (resp. $s_2^{(2p+2)}$) if $af^{2p+1} < 1$ (resp. $af^{2p+2} > 1$), because of the alternation of maxima and minima. In conclusion, $s^{(2p)}$ has as many extrema as s_1 (resp. s_2) if $af^{2p+1} < 1$ (resp. $af^{2p+2} > 1$).

■

ACKNOWLEDGEMENT

The authors would like to thank anonymous reviewers for having helped to improve the general presentation of the document.

REFERENCES

[1] N. Huang, Z. Shen, S. Long, M. Wu, H. Shih, Q. Zheng, N. Yen, C. Tung, and H. Liu, "The empirical mode decomposition and the Hilbert spectrum for nonlinear and non-stationary time series analysis," *Proceedings of the Royal Society : Mathematical, Physical and Engineering Sciences*, vol. 454, no. 1971, pp. 903–995, 1998.

[2] P. Flandrin, P. Gonçalves, and G. Rilling, "Detrending and denoising with empirical mode decompositions," in *Proceedings of Eusipco*, Wien (Austria), 2004, pp. 1581–1584.

[3] K. Coughlin and K. Tung, "11-year solar cycle in the stratosphere extracted by the empirical mode decomposition method," *Advances in space research*, vol. 34, no. 2, pp. 323–329, 2004.

[4] E. Delechelle, J. Lemoine, and O. Niang, "Empirical mode decomposition: an analytical approach for sifting process," *IEEE Signal Process. Lett.*, vol. 12, no. 11, pp. 764–767, 2005.

[5] S. El Hadji, R. Alexandre, and A. Boudraa, "Analysis of Intrinsic Mode Functions: A PDE Approach," *IEEE Signal Process. Lett.*, vol. 17, no. 4, pp. 398–401, 2010.

[6] S. Peng and W. Hwang, "Adaptive signal decomposition based on local narrow band signals," *IEEE Trans. Signal Process.*, vol. 56, no. 7 Part 1, pp. 2669–2676, 2008.

[7] S. Meignen and V. Perrier, "A new formulation for empirical mode decomposition based on constrained optimization," *IEEE Signal Process. Lett.*, vol. 14, no. 12, pp. 932–935, 2007.

[8] G. Rilling, P. Flandrin, and P. Gonçalvès, "On empirical mode decomposition and its algorithms," in *IEEE-EURASIP workshop on nonlinear signal and image processing NSIP-03, Grado (I)*, 2003.

[9] R. Sharpley and V. Vatchev, "Analysis of the intrinsic mode functions," *Constructive Approximation*, vol. 24, no. 1, pp. 17–47, 2006.

[10] P. Flandrin, G. Rilling, and P. Goncalves, "Empirical mode decomposition as a filter bank," *IEEE Signal Process. Lett.*, vol. 11, no. 2, pp. 112–114, 2004.

[11] H. Hong, X. Wang, and Z. Tao, "Local Integral Mean-Based Sifting for Empirical Mode Decomposition," *IEEE Signal Process. Lett.*, vol. 16, no. 10, p. 841, 2009.

[12] C. De Boor, *A practical guide to splines*. Springer-Verlag, New York, 1978.

[13] H. Prautzsch, W. Boehm, and M. Paluszny, *Bézier and B-spline techniques*. Springer Verlag, 2002.

[14] Y. Kopsinis and S. McLaughlin, "Investigation and performance enhancement of the empirical mode decomposition method based on a heuristic search optimization approach," *IEEE Trans. Signal Process.*, vol. 56, no. 1, pp. 1–13, 2007.

[15] G. Rilling and P. Flandrin, "One or two frequencies? The empirical mode decomposition answers," *IEEE Trans. Signal Process.*, vol. 56, no. 1, pp. 85–95, 2008.

[16] N. Stevenson, M. Mesbah, and B. Boashash, "A sampling limit for the empirical mode decomposition," in *Signal Processing and Its Applications, 2005. Proceedings of the Eighth International Symposium on*, vol. 2, 28-31, 2005, pp. 647 – 650.

[17] Q. Chen, N. Huang, S. Riemenschneider, and Y. Xu, "A B-spline approach for empirical mode decompositions," *Advances in Computational Mathematics*, vol. 24, no. 1, pp. 171–195, 2006.

[18] T. Oberlin and S. Meignen, http://www-ljk.imag.fr/membres/Thomas.Oberlin/EMDOS.tar.gz, 2011.

[19] S. Olhede and A. Walden, "The Hilbert spectrum via wavelet projections," *Proceedings of the Royal Society of London. Series A: Mathematical, Physical and Engineering Sciences*, vol. 460, no. 2044, p. 955, 2004.

[20] Y. Kopsinis and S. McLaughlin, "Development of EMD-based denoising methods inspired by wavelet thresholding," *IEEE Trans. Signal Process.*, vol. 57, no. 4, pp. 1351–1362, 2009.

[21] D. Donoho and J. Johnstone, "Ideal spatial adaptation by wavelet shrinkage," *Biometrika*, vol. 81, no. 3, p. 425, 1994.

[22] R. Deering and J. Kaiser, "The use of a masking signal to improve empirical mode decomposition," in *Acoustics, Speech, and Signal Processing, 2005. Proceedings. (ICASSP '05). IEEE International Conference on*, vol. 4, march 2005, pp. iv/485 – iv/488 Vol. 4.

[23] Z. Wu and N. Huang, "Ensemble empirical mode decomposition: A noise-assisted data analysis method," *Advances in Adaptive Data Analysis*, vol. 1, no. 1, pp. 1–41, 2009.

[24] C. Damerval, S. Meignen, and V. Perrier, "A fast algorithm for bidimensional EMD," *IEEE Signal Process. Lett.*, vol. 12, no. 10, pp. 701–704, 2005.